Metal-Assisted Plasma Etching of Silicon: A Liquid-Free Alternative to MACE

Julia B. Sun and Benjamin D. Almquist*

Department of Bioengineering, Imperial College London, London SW7 2AZ United Kingdom

ABSTRACT: For decades, fabrication of semiconductor devices has utilized well-established etching techniques to create complex nanostructures in silicon. Of these, two of the most common are reactive ion etching in the gaseous phase and metal-assisted chemical etching (MACE) in the liquid phase. Though these two methods are highly established and characterized, there is a surprising scarcity of reports exploring the ability of metallic films to catalytically enhance the etching of silicon in dry plasmas via a MACE-like mechanism. Here, we discuss a metal-assisted plasma etch (MAPE) performed using patterned gold films to catalyze the etching of silicon in an SF_6/O_2 mixed plasma, selectively increasing the rate of etching by over 1000%. The degree of enhancement as a function of Au catalyst configuration and relative oxygen feed concentration is characterized, along with the catalytic activities of other common MACE metals including Ag, Pt, and Cu. Finally, methods of controlling the etch process are briefly explored to demonstrate the potential for use as a liquid-free fabrication strategy.

INTRODUCTION

Silicon (Si) has long been the cornerstone material in the modern semiconductor industry, establishing a wealth of fabrication techniques in Si processing. The impressive diversity in fabricated Si nanostructures is galvanizing the expansion of Si to wide-ranging industries from photovoltaics to biotechnology. Recent applications of Si nanostructures include photonics[1], solar energy conversion[2], thermoelectric conversion[3], energy storage[4,5], catalysis[6–8], chemical and biochemical sensing[9–11], drug delivery[12], and biological imaging[13]. These diverse applications have driven the development and optimization of a variety of methods for controlling the fabrication of Si structures, ranging from the early years of wet chemical etching before the 1970s, followed by the development of reactive ion etching (RIE) in the mid-1970s. Each method has been expanded on over the years, with the 1990s providing two major additions: metal-assisted chemical etching (MACE) for wet etching and deep reactive ion etching (Bosch process) for dry etching.

Since the first report of MACE in 1997, the technique has grown exponentially due to its simplicity and cost effectiveness[14–17]. In MACE, Si substrates are deposited with catalytic layers of noble metals such as Au, Ag, Pt, and Pd[18–27] and immersed in an aqueous etchant of hydrofluoric acid (HF) and an oxidative agent such as hydrogen peroxide (H_2O_2). Si covered by the noble metal catalyst etches significantly faster than uncovered Si, transferring the pattern of the deposited metal catalyst to the underlying Si. Additional metals such as Cu, W, and Ni[28–31] have also been shown to exhibit MACE but with lower efficacy than noble metals. This straightforward approach to highly selective Si etching has supported the wide uptake of MACE as a fabrication strategy.

Although the exact mechanism of MACE is still under debate, there is a general consensus that MACE proceeds through electrochemical and mass transport reactions[15,32–35]. The oxidant, H_2O_2, is transported and reduced at the surface of the catalytic metal (Figure 1). This reaction causes electrons to be extracted from the underlying Si, thus injecting holes, to create electron-poor depletion regions in Si that are more susceptible to etching by HF. For thin metal layers, pores generated in the metal during etching facilitate transport of the HF through the film to enable etching of the underlying oxidized Si, with reactant byproducts carried away in solution[36]. For thick metal layers, this process happens at the Si/metal interface. Since the depletion regions concentrate at the Si/metal interface, HF etches the metal-masked Si faster than exposed Si. The high catalytic ability of noble metals to reduce O_2 and H_2O_2[37–42] and reduction potential differences between the catalytic metal and Si[36] are theorized to be major driving forces in the mechanism of MACE.

While a significant body of literature has explored the process and controllability of MACE, there is a relative lack of previous studies investigating how metals can be used to enhance etching in plasmas. Mask-enhanced etching of Si and SiO_2 using Al, Cr, Cu, and Ag masks is known in fluorine-containing etch chemistries[43–46]; the increased etch rates for Si with metal masking is attributed to local increases in fluorine concentration due to the catalytic production of fluorine radicals on the surface of the metal mask. In one report, Au placed upstream of the substrate was shown to increase downstream Si etch rate by 3.6 times in CF_4/O_2 plasma, with the increased etch rate attributed to gas phase transport of Au oxides and fluorine radicals to the substrate[47]. In contrast to Au, Ag and Pt did not have a similar effect, despite Ag demonstrating mask-enhanced etching[45]. In other research, Cu deposits on Si enhance the Si etch rate in F_2 and Cl_2 by catalyzing fluorination and chlorination reactions of Si, respectively[48,49]. Also, one study reports enhanced etching of Si underneath Ag, but not under Au, in CF_4/O_2 plasmas[50]. This finding is contradicted by two subsequent studies that demonstrate Au indeed enhances the etching of Si in CF_4/O_2, with the authors suggesting, in agreement with mask-enhanced etching, that the observed effects are due to an increase in the production of fluorine radicals within the vicinity of the Au[51,52].

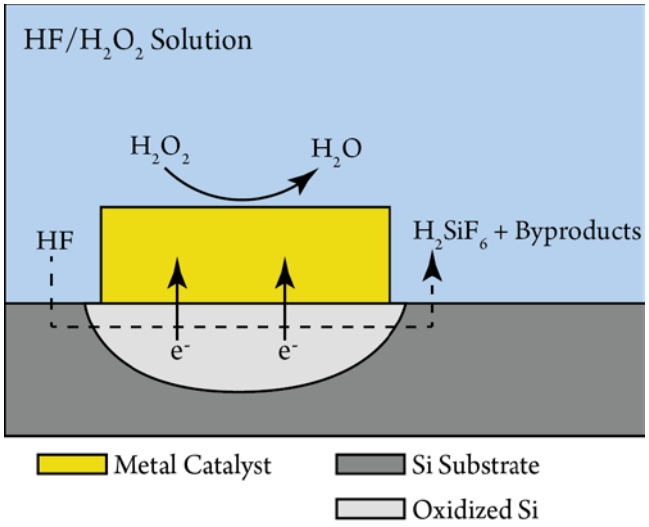

Figure 1. Mechanism of MACE. When metal catalyst patterned on a Si substrate is exposed to HF/H_2O_2, the metal reduces H_2O_2 and withdraws electrons from the underlying Si. Transport of HF to the metal/Si interface causes HF to react with oxidized Si and facilitates the enhanced etching of Si.

However, outside of these limited studies, there has been a shortage of exploration regarding the details of how metals can catalyze Si etching in reactive plasmas, and if it is merely due to an increase in fluorine radicals or potentially operates via a MACE-like mechanism. Here, we explore the use of metal-assisted plasma etching (MAPE) as a liquid-free method for etching Si in an RIE system. Metallic film nanostructures are patterned onto Si substrates to catalyze the enhanced etching of Si in an SF_6/O_2 mixed plasma. We observe etch rates that are over 1000% higher than the expected rate for Si and proceed through a mechanism of enhancement that relies on direct Si contact with the metal, does not increase the etch rate of proximal Si, and provides an increase of the etch rate on par with that of MACE. Furthermore, this effect differs from enhanced etching at mask edges created by diffusion-limited reactions and allows for the creation of anisotropic profiles that reproduce the patterned metallic nanostructures. In turn, MAPE is an intriguing technique for liquid-free metal-assisted etching of high-aspect-ratio silicon micro- and nanostructures.

EXPERIMENTAL METHODS

Patterning of Periodic Arrays: Nanostructures were patterned onto p- and n-type (100) silicon wafers with resistivity 1-10 Ω cm (Pi-Kem, UK) spin-coated with polymethyl methacrylate 950-A2 (Microchem, USA), and patterned using a RAITH 150 TWO electron beam lithography system (Raith GmbH, Germany). Following exposure, patterns were developed in a 1:3 mixture of methyl isobutyl ketone in isopropyl alcohol and treated in oxygen plasma in a Diener plasma generator (Diener electronic GmbH & Co. KG, Germany) to remove excess photoresist scum and produce final circular features with an approximate diameter of 200 nm. Microstructures were patterned onto silicon wafers spin-coated with S1805 photoresist (Microchem, USA) using phase shift lithography. A borosilicate mask etched with lines 1.5 inches in length and 1.5 μm thick with 1.5 μm spacing was used to perform double exposures at 5 mJ/cm^2 with the mask turned 90° in between exposures on a Quintel Q4000-6 Mask Aligner (Neutronix Quintel, USA). Patterns were developed in MICROPOSIT MF-26A (Dow Electronic Materials, USA) to produce final rectangular patterns measuring approximately 1 μm by 1.3 μm.

Thin Film Deposition: After patterning, layers of Au and other metals were deposited in an Edwards A500-FL500 electron beam metal evaporator (Edwards High Vacuum International, UK) to form thin layers ranging from 5 nm to 25 nm in thickness. Uniformity was confirmed using a DektakXT surface profilometer (Bruker Corporation, USA). Lift-off of excess photoresist and metals was performed using MICROPOSIT Remover 1165 solvent (Dow Electronic Materials, USA).

RIE: The masked silicon wafers were etched in a parallel plate PlasmaPro NGP90 plasma processing system (Oxford Instruments, UK). Reactive ion etching was performed at 175 mTorr using a forward power of 50 W, and the total gas flow of SF_6/O_2 was held constant at 40 sccm. The total concentration of O_2 was varied by changing the relative gas flow rates of SF_6 and O_2.

Imaging: Visualization of the etched structures was performed with regular and tilting SEM on a Zeiss XB1540 (Carl Zeiss AG, Germany) and LEO Gemini 1525 FEGSEM (LEO Electron Microscopy Inc, USA). Tilting images were executed at 45° for etched structure imaging and 90° for side fractural imaging.

Etch Enhancement Measurements: Si substrates following plasma treatment were fractured for cross-sectional imaging of the etch pits. The vertical etch depth was measured at the center of the Si pillars or catalytically etched pits using ImageJ. Ten measurements were made for every 12x12 nanostructured array. The etch enhancement over 0% O_2 was measured by normalizing each measured value to the mean value for the Si substrate treated at 0% O_2. For substrates that formed etch pits, the mean value at 0% O_2 was added to the vertical etch measurement to account for the trenching effect.

RESULTS AND DISCUSSION

Metal-Assisted Plasma Etching. To explore the use of MAPE in SF_6-based plasmas, nano- and microstructure arrays were patterned using electron beam and phase shift lithography on n-type and p-type (100) silicon substrates with resistivity 1-10 Ω cm. Thin films of Au (5 nm) were deposited using electron beam metal evaporation. A thin film of Cr (10 nm) was deposited on top of the Au film to protect Au from physical etching, creating bi-layered metallic nanostructures (Figure 2a). Cr was chosen due to its high etch resistance in fluorine-based plasmas[53]. Following solvent lift-off to expose the underlying Si, patterned arrays were subjected to RIE etching with mixed SF_6/O_2 gas chemistries for 3 minutes.

Under normal conditions, SF_6-based plasma isotropically etches exposed Si to create Si nanopillars underneath each masking structure[54]. However, when the bilayer Au/Cr catalytic structures are etched, areas of Si covered by the patterned metal exhibit preferential and enhanced etching far exceeding the expected etch rates of Si (Figure 2b, S1). This enhanced etching gives rise to deep trenches at the original location of each metallic structure, with the boundaries of the etching extending outside those of the original metal structure, but confined locally to the array of the 12x12 metal dots. This enhanced etching is seen in both p-type and n-type silicon, suggesting the etch enhancement is intrinsic to the Si and not dependent on the type of substrate doping (Figure 2c).

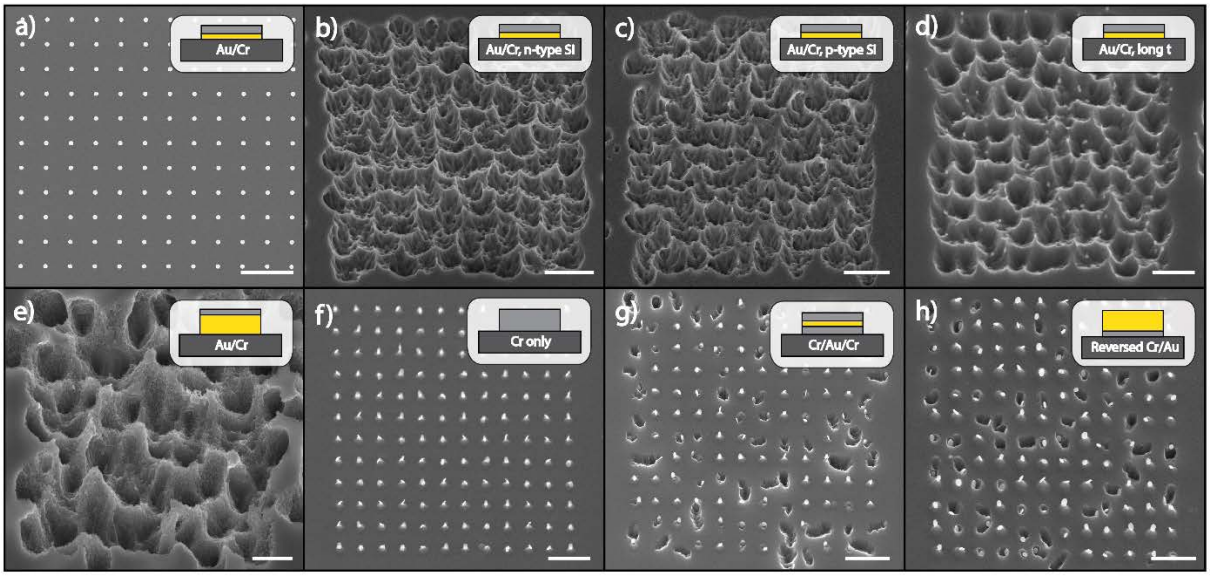

Figure 2. Metal-assisted plasma etching of Si. a) Thin films of 5 nm Au and 10 nm Cr were patterned by electron beam lithography onto Si substrates in 12x12 circular nanostructured arrays. Each nanostructure measured 200 nm in diameter. All scale bars represent 2 μm. b) N-type Si substrates patterned with Au/Cr nanostructures were treated for 3 minutes in a mixed SF_6/O_2 plasma at 25% O_2 concentration. Deep etch trenches characteristic of localized catalytic etching formed underneath each nanostructure while exposed Si at the edges of the array did not exhibit catalytic etching. c) P-type Si substrates patterned and treated at the same conditions produced no significant difference in etching when compared to the n-type Si substrates. d) Si substrates patterned with Au/Cr exhibited similar enhanced etch profiles after etching for 6 minutes. e) A thicker film of 25 nm Au was patterned onto Si substrates with 10 nm Cr on top. After plasma treatment, etched substrates presented a higher degree of etch enhancement with more pronounced etch trenches due to the increased Au film. f) Circular Cr-only (25 nm) nanostructures were patterned on Si substrates and subsequently treated in SF_6/O_2 for 3 minutes. Si pillars formed underneath each Cr masking nanostructure and exhibited no evidence of enhanced etching with the removal of the catalytic Au layer. g) Sandwich architecture nanostructures were created by depositing 5 nm Au in between 10 nm layers of Cr. Si substrates with this architecture showed a notable decrease in catalytic etching. Enhanced etch pits occurred only where nanostructures tilted in an orientation to allow the middle Au layer to contact the Si substrate. h) A reverse architecture of 10 nm Cr and 25 nm Au was patterned onto Si substrates. After plasma treatment, a similar catalytic inhibition occurs with Cr serving as an etch stop only when the orientation of the particle results in isolation of the Au from the Si.

To further understand the mode of etch enhancement, the length of plasma treatment and metal film thickness were varied in the etch experiments. Interestingly, Si substrates patterned with the same bilayer metal structure but etched for twice as long (6 minutes) in plasma exhibit no noticeable difference to those etched for 3 minutes (Figure 2d). At these testing conditions, the etch enhancement does not appear to increase with increasing time. Furthermore, nanostructures with a thicker Au film (25 nm Au/10 nm Cr) produce pronounced etch features in the Si that are deeper and rougher than thinner Au films (Figure 2e). The amount of enhanced etching increases with the increased thickness of Au, suggesting that Au is the main catalytic reagent enabling the metal-enhanced etching of Si, and that the process of enhanced etching likely consumes it. Taken together, the extent of etching appears to depend primarily on the amount of Au, with higher amounts of Au enhancing etching for a longer time before being consumed. Cr-only nanostructures do not display this enhanced etching, supporting the critical role of Au in catalyzing the MAPE process (Figure 2f).

To determine whether the direct Au-Si contact is necessary to facilitate MAPE, we constructed two different configurations of metal films. First, a thin Au layer was deposited between two layers of Cr to create a sandwich architecture (10 nm Cr/5 nm Au/10 nm Cr), isolating the catalytic layer and preventing its contact with the underlying Si. The etched Si substrates exhibited a notable decrease in MAPE with many Si areas forming pillars underneath the nanostructures, although some regions still form the unmistakable trenches from enhanced etching (Figure 2g). Examination of the nanostructures that maintained the enhanced etch profile suggests that Au-Si contact is essential since these nanostructures became oriented in a way that allowed the exposed edge of the sandwiched Au layer to contact the Si surface (Figure S1, S2). To further test this concept, a second film configuration was made by placing a thick Au layer (25 nm) above a Cr film (10 nm). In agreement with the sandwich structure, this reverse configuration led to a significant reduction in MAPE, with cases of enhanced etching again occurring only where the nanoparticles appear to reorient themselves so that the top Au layer contacts the Si (Figure 2h, S2).

These data suggest that Au is unable to diffuse through the Cr layer to the underlying Si to facilitate etching. Furthermore, there is little evidence that etched Au or fluorine radicals produced on the surface are transported through the plasma or diffuse on top of Cr; the trenches due to enhanced etching localize only to the areas patterned with nanostructures following reorientation that places Au in direct contact with Si. If transport of Au of fluorine radicals in the plasma occurs, enhanced etching should be visible in the proximity of the nanoparticles without direct contact between the Au and Si. However, these experiments find that no enhanced etching is observed even within nanometers of Au particles unless there is direct contact between Au and Si. Finally, it is interesting to note that the extent of etching is similar between the sandwich structure (Figure

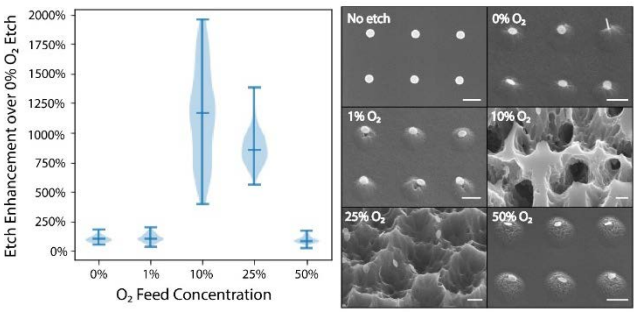

Figure 3. Effect of O_2 concentration on MAPE. Si substrates were patterned with 5 nm Au/10 nm Cr and etched for 3 min in SF_6/O_2. By maintaining the total flow rate at 40 sccm and manipulating the O_2 flow rate, we examined the effect of O_2 concentration on the etch enhancement over a 0% O_2 etch. (left) Violin plots indicating the median and range for each condition. Little or no etch enhancement was measured at 0% and 1% O_2 while treatment in 10% O_2 exhibited a maximal amount of catalytic enhancement. A smaller degree of etch enhancement occurs at 25% O_2 with the disappearance of etch enhancement at 50% O_2. (right) Representative images of etching. All scale bars are 400 nm.

2g) and inverse structure (Figure 2h), despite the inverse structure having an exposed Au surface area that is over 10x larger than the sandwich structure. This lack of dependence on surface area further supports the concept that the surface of the Au does not generate diffusible products that facilitate the increase in etch rate, and that direct contact between the Au and Si is necessary for enhancing the rate of etching.

From this data, several conclusions are possible regarding the mechanism of MAPE. First, Au acts as a catalytic reagent to promote the enhanced etching of Si in SF6/O2 plasma. The enhanced etching effect is far more pronounced than typical Si etching. Second, direct contact of Au on Si is critical for the catalytic etching reaction to proceed. The enhanced etching can be blocked by entirely isolating the Au layer from the Si surface with a non-reactive metal like Cr. Third, the degree of enhancement depends on the amount of catalytic Au present, suggesting that the mechanism likely consumes Au. In these experiments, the amount of remaining Au measured on the Si substrates following etching was less than the detection limit for energy-dispersive X-ray spectroscopy. If the etch is well controlled, it appears that MAPE has the potential to operate as a self-limiting etch that terminates after depletion of the Au catalyst. This aspect is different from MACE where the catalytic metal remains on the etched substrate and the etch process ends by manual removal of the substrate or neutralization of the chemical etchants. Note that although it appears that MAPE consumes the Au, it is referenced here as a metal catalyst due to the analogous enhancement of Si etching to metal catalysts in MACE. Finally, transport of the plasma ions to the Au/Si interface is required. Data from Si substrates patterned with large lateral Au/Cr bilayer structures of the same thickness (5 nm Au/10 nm Cr) and etched in SF_6/O_2 further supports this requirement (Figure S3). Si substrates exhibit similar enhanced etching to the nanopatterned substrates, but only at the Au/Si/plasma interfaces. Furthermore, images from early etching with nanoparticles suggests that pillars created via conventional SF_6/O_2 plasma etching precede metal-enhanced etching (Figure S4), with enhanced etching likely starting following exposure of the Au-Si interface to the plasma. Importantly, the metal nano- and microstructures

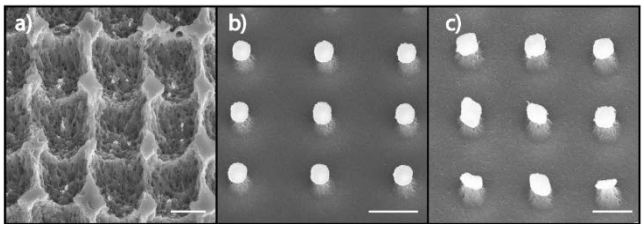

Figure 4. MACE metals in MAPE. a) Microstructure arrays patterned by phase shift lithography on Si substrates. 25 nm of Ag was deposited onto the substrate to form 1.0 x 1.3 μm rectangular structures. After treatment in an SF_6/O_2 plasma for 3 min, Si substrates exhibited etch profiles indicative of MAPE. Little of the Ag microstructures remained in the etch trenches, likely due to the low resistance of Ag to etching in SF_6 plasmas. b) Similar microstructures were created with 25 nm Pt. After treatment, Si pillars formed underneath each Pt microstructure with no evidence of enhanced etching. c) Si substrates patterned with 25 nm Cu also did not exhibit MAPE after plasma treatment although the etch produced increased roughness on the Si surface. All scale bars are 2 μm.

catalyze an enhanced etching phenomenon that is divergent from plasma-enhanced edge effects. Catalytic activity is not purely limited to the mask edges from a concentration of reactive species on the mask or enhancement of the field strength. Instead, the Au in direct contact with Si actively promotes enhanced etching in SF_6/O_2 plasmas.

Effects of Oxygen Content on MAPE. Having established that SF_6-based plasmas facilitate MAPE, we then aimed to determine the impact of oxygen in the process. The addition of O_2 to SF_6 is known to increase the F-atom concentration, increasing overall Si etch rate by preventing the recombination of F atoms with SF_x radicals through the formation of SO_2 and SOF_4[55]. To determine if MAPE maintains this O_2 dependence, we evaluated a range of O_2 concentrations from 0% to 50% at a constant total flow rate and pressure (Figure 3, S5). Minimal or no MAPE occurs when the fraction of O_2 is 1% or less, whereas at 10% O_2 we observe the maximum enhancement of the MAPE process. This finding follows a similar trend to previous reports of maximal Si etch rates occurring between 10-40% O_2 composition for both SF_6/O_2 and CF_4/O_2 etch chemistries[56–58], though the maximum etch rate has been known to vary based on system-specific parameters[55].The MAPE process is observed through 25% O_2 but exhibits a significant decrease at 50% O_2. This decrease is supported by previous observations of an inversion in etch rates above 40% O_2 due to competitive adsorption of increasing oxygen species onto Si reaction sites over fluorine species[56]. Taken together, these data suggest that similar to its effect on normal Si etch rates for fluorine/oxygen plasmas, the relative concentration of O_2 in the plasma plays a significant role in determining the etch rate of MAPE.

Translation of Additional MACE Metals to MAPE. In addition to Au, liquid phase MACE is routinely achieved using other noble metals such as Ag and Pt, and to a lesser degree, Cu. To determine if the catalytic effect is transferrable to MAPE, Si substrates were patterned with microstructures of the common MACE catalysts Ag, Pt, and Cu and etched using the same conditions as those in Figure 2. Similar to substrates patterned with Au films, Si substrates patterned with Ag films exhibit enhanced etching suggesting Ag has a comparable ability to facilitate MAPE (Figure 4a). However, substrates patterned with Pt do not show increased etching of the Si substrate (Figure 4b) despite Pt MACE being faster

than Au MACE[18]. Substrates patterned with Cu also do not exhibit any catalytic etching but instead induce a rougher Si surface following etching than Pt (Figure 4c).

The difference in the catalytic effect between MACE and MAPE suggests the mechanism of MAPE deviates from that of MACE, although the exact reason why a metal will function as a catalyst in MACE but not MAPE is not currently fully understood. Unlike in MACE where the reduction potential of the metal catalyst in relation to the Si ionization potential predicts whether a metal will function as a MACE catalyst[36], reduction potential does not correctly predict the non-catalytic behavior of Pt and Cu in MAPE. Although shown not to correlate with MACE activity, previous studies have demonstrated that changing the work function of metals can enhance their catalytic activity[59]. In agreement with MACE findings, measurements of the work function of catalyst-only and catalyst/Cr configurations do not demonstrate an accurate prediction model for MAPE (Figure S6).

The diffusion of metals into Si substrates and the reverse diffusion of Si into metal is fast even at modest temperatures[60]. Increased diffusion at the metal/Si interface may facilitate enhanced Si etching by increasing the overall mobility of metal ions and their ability to modulate the electron density of Si[61]. This contradicts the mechanism underpinning MACE, where the catalytic metals serve to extract electrons/inject holes and neither the Si nor metal noticeably enriches with diffused atoms. Though the diffusivities of Pt and Cu do not significantly differ from the diffusivities of Au and Ag on Si[62], the formation of metal oxides on the surface of the catalyst metal when exposed to O_2 and/or the ability to form stable compounds with Si, as opposed to solid solutions, may provide insight into a possible mechanism. Binary oxides formed from Pt and Cu have higher thermodynamic stability when compared to oxides formed from Au and Ag on Si[63]. Since MAPE occurs in the presence of O_2, the increased stability of these oxides may negatively impair the diffusion at the metal/Si interface[64], in turn inhibiting the enhanced etching. Furthermore, Pt/Si and Cu/Si readily form stable compounds[64,65], potentially reducing their ability to act as Si oxidizing agents.

An alternative mechanism underpinning the enhanced etching is the possible formation of surface-associated metal fluorides. Metal fluoride compounds such as AuF_5, AgF_2, and AgF_3 are known to be strong oxidizing agents[66–68] and may draw electrons from Si to create active sites for etching. These metal fluorides form when the metal surface is exposed to fluorine species in plasma and may more readily compete with the formation of metal oxides due to increased thermodynamic stability[69]. High electron affinity metal fluorides formed with Pt are possible, but compounds such as PtF_6 are known to be volatile at room temperature[70], potentially resulting in rapid removal from the Si-Pt interface. Overall, this mechanism that relies on the production of metal fluorides to oxidize underlying Si is similar to the MACE mechanism wherein the metal catalyst serves to oxidize underlying Si for etching.

Therefore, based on the data presented here we propose the following potential MAPE mechanism (Figure 5): (1) The generation of an SF_6/O_2 plasma creates reactive species including F and O radicals, SO_2F_2, SOF_4, and other charged species. (2) Diffusion occurs across the metal/Si interface as metal ions diffuse into the underlying Si and Si atoms diffuse through the metal layer to the surface. (3)

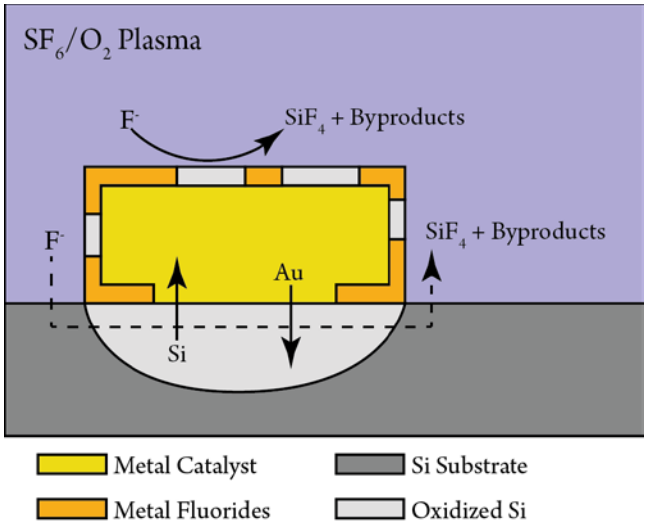

Figure 5. The proposed mechanism of MAPE. Diffusion occurs across the Si – metal interface, resulting in oxidation of both the Si underlying the metal and Si diffusing to the surface of the metal. In the presence of SF_6/O_2 plasma, surface-associated metal fluorides form that further oxidize the Si. Fluorine radicals present in the plasma etch the oxidized Si at a faster rate than standard Si.

Si is oxidized on the surface of the metal or by electron density modulation by dissolved metal ions in the underlying Si. In addition, the surface of the metal chemically reacts with fluorine species to form metal fluoride oxidizing agents. The surface associated metal fluorides oxidize the underlying Si at the metal/Si interface. Finally, (4) the etching reaction proceeds with the transport of fluorine species to the oxidized Si, the formation of SiF_4 products, and subsequent removal of byproducts via the plasma. Similar to liquid phase MACE, MAPE likely proceeds through both redox and mass transport reactions. However, further investigation is essential to fully understand the underpinning mechanism and establish a predictive model for catalytic metal activity in dry plasmas.

Controlling the Process of MAPE. The applicability of MAPE depends on the ability to control the process during etching. To this end, we demonstrate the ability to control catalytic etching by pulsing the plasma to form selective etch pits (Figure 6). By generating a plasma and allowing the reaction to proceed for a shorter amount of time (1 minute or less), it is possible to limit the extent of catalytic etching so that the Si trenches more closely resemble the original size of the patterned metallic structures (Figure 6a-b). Time pulsing is hypothesized to act as a method of control by limiting the MAPE reaction, thus reducing the distance of diffusion or limiting the chemical formation of metal fluorides, to enable a more localized reaction at the metal/Si interface. Using this method, it is possible to form large areas of uniform lattice structures by etching Si substrates with patterned microstructures (Figure 6c-d). Through refinement of the temporal pulsing method, it may be possible to use MAPE to create complex, high-aspect-ratio micro- and nanostructures. Alternatively, nanostructures patterned on a thermally grown SiO_2 film do not exhibit enhanced etching, suggesting that oxide formation impedes MAPE (Figure S7). This feature may permit the use of O_2 plasma treatment steps in between fluorine-based etch steps to grow protective oxide barrier layers for improved fabrication control.

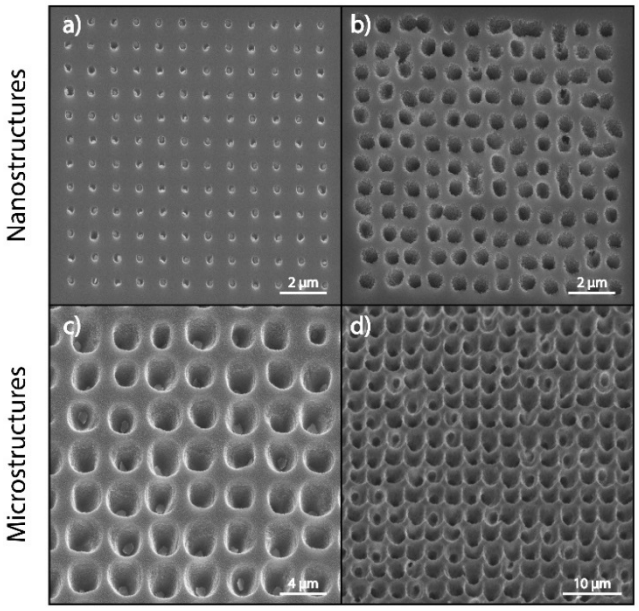

Figure 6. Time pulsing as a method of control for nano- and microstructures. a) Si substrates patterned with 5 nm Au/10 nm Cr nanostructured arrays were etched for 1 minute to create a limited local etch where the Si substrate contacted each nanostructure. b) Substrates with the same nanostructure architecture were treated for two cycles of 1 minute each to produce deeper etch trenches that more faithfully reproduced the shape of the catalytic nanostructures. c) The method of pulsed time control extends to catalytic microstructures. Si substrates patterned with microstructures of 5 nm Au/10 nm Cr exhibited controlled etch trenches after similar plasma treatment (2x1 min). d) Si substrates patterned with microstructures and treated for two cycles of 1 min followed by a 4 min cycle produced uniform patterns of deep lattice structures across the entire substrate.

CONCLUSION

In summary, we have explored a MACE-like effect in dry SF_6/O_2 plasmas by utilizing patterned metallic nano- and microstructures to catalytically enhance the etch rate of silicon. Direct contact between the metal catalyst and Si substrate is necessary for this localized etch effect, and diverges from enhanced mask edge etching due to the higher degree of enhancement for all areas of underlying Si contacting the metal nanostructure. The MAPE process exhibits a rate dependence on oxygen feed concentration similar to that of classic silicon etching. Interestingly, not all metals that function as MACE catalysts can function as MAPE catalysts, indicating that the plasma-based mechanism deviates from that of liquid phase MACE. Crucially, preliminary results suggest that methods of control including temporal pulsing and oxide barrier formation are possible, and are shown to enable the creation of uniform lattice structures with relative processing ease. Importantly, limitations of liquid phase MACE such as fluid flow effects, stiction, and solute deposition are not present with MAPE. With further development of the techniques described here, MAPE may provide an exciting strategy for high-aspect-ratio Si processing in liquid-free environments.

ASSOCIATED CONTENT

Supporting Information. This material is available free of charge via the Internet at

AUTHOR INFORMATION

Corresponding Author

*Email: b.almquist@imperial.ac.uk

ORCID

Julia B. Sun: 0000-0001-9768-4362
Benjamin D. Almquist: 0000-0001-9718-777X

Author Contributions

JBS and BDA conceived the research and planned the experiments. JBS performed the experiments. JBS and BDA analyzed the data. JBS and BDA wrote the manuscript.

Notes

The authors declare no competing financial interests.

ACKNOWLEDGMENT

This research was supported by Wellcome Trust grant 109838/Z/15/Z and the Department of Bioengineering at Imperial. J.B.S. acknowledges the Imperial College London Presidential PhD Scholarship fund. The authors thank Matyas Daboczi for assistance with Kelvin Probe measurements, along with Dr Firat Güder and Dr Danny O'Hare for insightful discussions and suggestions.

REFERENCES

(1) Priolo, F.; Gregorkiewicz, T.; Galli, M.; Krauss, T. F. Silicon Nanostructures for Photonics and Photovoltaics. *Nat. Nanotechnol.* **2014**, *9* (1), 19–32.

(2) Yu, P.; Wu, J.; Liu, S.; Xiong, J.; Jagadish, C.; Wang, Z. M. Design and Fabrication of Silicon Nanowires towards Efficient Solar Cells. *Nano Today* **2016**, *11* (6), 704–737.

(3) Schierning, G. Silicon Nanostructures for Thermoelectric Devices: A Review of the Current State of the Art. *Phys. status solidi* **2014**, *211* (6), 1235–1249.

(4) Ashuri, M.; He, Q.; Shaw, L. L. Silicon as a Potential Anode Material for Li-Ion Batteries: Where Size, Geometry and Structure Matter. *Nanoscale* **2016**, *8* (1), 74–103.

(5) Zuo, X.; Zhu, J.; Müller-Buschbaum, P.; Cheng, Y.-J. Silicon Based Lithium-Ion Battery Anodes: A Chronicle Perspective Review. *Nano Energy* **2017**, *31*, 113–143.

(6) Yang, X.; Zhong, H.; Zhu, Y.; Jiang, H.; Shen, J.; Huang, J.; Li, C. Highly Efficient Reusable Catalyst Based on Silicon Nanowire Arrays Decorated with Copper Nanoparticles. *J. Mater. Chem. A* **2014**, *2* (24), 9040.

(7) Wang, F.; Shao, M.; Cheng, L.; Chen, D.; Fu, Y.; Ma, D. D. D. Si/Pd Nanostructure with High Catalytic Activity in Degradation of Eosin Y. *Mater. Res. Bull.* **2009**, *44* (1), 126–129.

(8) Casiello, M.; Picca, R. A.; Fusco, C.; D'Accolti, L.; Leonardi, A. A.; Lo Faro, M. J.; Irrera, A.; Trusso, S.; Cotugno, P.; Sportelli, M. C.; et al. Catalytic Activity of Silicon Nanowires Decorated with Gold and Copper Nanoparticles Deposited by Pulsed Laser Ablation. *Nanomaterials* **2018**, *8* (2), 78.

(9) Harraz, F. A. Porous Silicon Chemical Sensors and Biosensors: A Review. *Sensors Actuators B Chem.* **2014**, *202*, 897–912.

(10) Ozdemir, S.; Gole, J. L. The Potential of Porous Silicon Gas Sensors. *Curr. Opin. Solid State Mater. Sci.* **2007**, *11*, 92–100.

(11) Wang, Y.; Wang, T.; Da, P.; Xu, M.; Wu, H.; Zheng, G. Silicon Nanowires for Biosensing, Energy Storage, and Conversion. *Adv. Mater.* **2013**, *25* (37), 5177–5195.

(12) Anglin, E. J.; Cheng, L.; Freeman, W. R.; Sailor, M. J. Porous Silicon in Drug Delivery Devices and Materials. *Adv. Drug Deliv. Rev.* **2008**, *60* (11), 1266–1277.

(13) He, Y.; Fan, C.; Lee, S.-T. Silicon Nanostructures for Bioapplications. *Nano Today* **2010**, *5* (4), 282–295.

(14) Dimova-Malinovska, D.; Sendova-Vassileva, M.; Tzenov, N.; Kamenova, M. Preparation of Thin Porous Silicon Layers by Stain

Etching. *Thin Solid Films* **1997**, *297* (1–2), 9–12.
(15) Huang, Z.; Geyer, N.; Werner, P.; de Boor, J.; Gösele, U. Metal-Assisted Chemical Etching of Silicon: A Review. *Adv. Mater.* **2011**, *23* (2), 285–308.
(16) Han, H.; Huang, Z.; Lee, W. Metal-Assisted Chemical Etching of Silicon and Nanotechnology Applications. *Nano Today*. 2014, pp 271–304.
(17) Li, X. Metal Assisted Chemical Etching for High Aspect Ratio Nanostructures: A Review of Characteristics and Applications in Photovoltaics. *Curr. Opin. Solid State Mater. Sci.* **2012**, *16* (2), 71–81.
(18) Li, X.; Bohn, P. W. Metal-Assisted Chemical Etching in HF/H2O2 Produces Porous Silicon. *Appl. Phys. Lett.* **2000**, *77* (16), 2572–2574.
(19) Zhang, M.-L.; Peng, K.-Q.; Fan, X.; Jie, J.-S.; Zhang, R.-Q.; Lee, S.-T.; Wong, N.-B. Preparation of Large-Area Uniform Silicon Nanowires Arrays through Metal-Assisted Chemical Etching. *J. Phys. Chem. C* **2008**, *112* (12), 4444–4450.
(20) Chartier, C.; Bastide, S.; Lévy-Clément, C. Metal-Assisted Chemical Etching of Silicon in HF–H2O2. *Electrochim. Acta* **2008**, *53* (17), 5509–5516.
(21) Kim, J.; Han, H.; Kim, Y. H.; Choi, S.-H.; Kim, J.-C.; Lee, W. Au/Ag Bilayered Metal Mesh as a Si Etching Catalyst for Controlled Fabrication of Si Nanowires. *ACS Nano* **2011**, *5* (4), 3222–3229.
(22) Tsujino, K.; Matsumura, M. Boring Deep Cylindrical Nanoholes in Silicon Using Silver Nanoparticles as a Catalyst. *Adv. Mater.* **2005**, *17* (8), 1045–1047.
(23) Tsujino, K.; Matsumura, M. Helical Nanoholes Bored in Silicon by Wet Chemical Etching Using Platinum Nanoparticles as Catalyst. *Electrochem. Solid-State Lett.* **2005**, *8* (12), C193–C195.
(24) Asoh, H.; Arai, F.; Ono, S. Effect of Noble Metal Catalyst Species on the Morphology of Macroporous Silicon Formed by Metal-Assisted Chemical Etching. *Electrochim. Acta* **2009**, *54* (22), 5142–5148.
(25) Yae, S.; Morii, Y.; Fukumuro, N.; Matsuda, H. Catalytic Activity of Noble Metals for Metal-Assisted Chemical Etching of Silicon. *Nanoscale Res. Lett.* **2012**, *7* (1), 352.
(26) Li, L.; Liu, Y.; Zhao, X.; Lin, Z.; Wong, C.-P. Uniform Vertical Trench Etching on Silicon with High Aspect Ratio by Metal-Assisted Chemical Etching Using Nanoporous Catalysts. *ACS Appl. Mater. Interfaces* **2014**, *6* (1), 575–584.
(27) Rykaczewski, K.; Hildreth, O. J.; Wong, C. P.; Fedorov, A. G.; Scott, J. H. J. Directed 2D-to-3D Pattern Transfer Method for Controlled Fabrication of Topologically Complex 3D Features in Silicon. *Adv. Mater.* **2011**, *23* (5), 659–663.
(28) Morinaga, H.; Suyama, M.; Ohmi, T. Mechanism of Metallic Particle Growth and Metal-Induced Pitting on Si Wafer Surface in Wet Chemical Processing. *J. Electrochem. Soc.* **1994**, *141* (10), 2834.
(29) Lee, J.-P.; Choi, S.; Park, S. Extremely Superhydrophobic Surfaces with Micro- and Nanostructures Fabricated by Copper Catalytic Etching. *Langmuir* **2011**, *27* (2), 809–814.
(30) Hildreth, O.; Alvarez, C.; Wong, C. P. Tungsten as a CMOS Compatible Catalyst for the Metal-Assisted Chemical Etching of Silicon to Create 2D and 3D Nanostructures. In *2010 Proceedings 60th Electronic Components and Technology Conference (ECTC)*; IEEE, 2010; pp 794–797.
(31) Yue, Z.; Shen, H.; Jiang, Y.; Wang, W.; Jin, J. Novel and Low Reflective Silicon Surface Fabricated by Ni-Assisted Electroless Etching and Coated with Atomic Layer Deposited Al2O3 Film. *Appl. Phys. A* **2014**, *114* (3), 813–817.
(32) Kim, J. D.; Mohseni, P. K.; Balasundaram, K.; Ranganathan, S.; Pachamuthu, J.; Coleman, J. J.; Li, X. Scaling the Aspect Ratio of Nanoscale Closely Packed Silicon Vias by MacEtch: Kinetics of Carrier Generation and Mass Transport. *Adv. Funct. Mater.* **2017**, *27* (12), 1605614.
(33) Li, L.; Zhao, X.; Wong, C.-P. Charge Transport in Uniform Metal-Assisted Chemical Etching for 3D High-Aspect-Ratio Micro- and Nanofabrication on Silicon. *ECS J. Solid State Sci. Technol.* **2015**, *4* (9), P337–P346.
(34) Lai, R. A.; Hymel, T. M.; Narasimhan, V. K.; Cui, Y. Schottky Barrier Catalysis Mechanism in Metal-Assisted Chemical Etching of Silicon. *ACS Appl. Mater. Interfaces* **2016**, *8* (14), 8875–8879.
(35) Hildreth, O. J.; Lin, W.; Wong, C. P. Effect of Catalyst Shape and Etchant Composition on Etching Direction in Metal-Assisted Chemical Etching of Silicon to Fabricate 3D Nanostructures. *ACS Nano* **2009**, *3* (12), 4033–4042.
(36) Kong, L.; Dasgupta, B.; Ren, Y.; Mohseni, P. K.; Hong, M.; Li, X.; Chim, W. K.; Chiam, S. Y. Evidences for Redox Reaction Driven Charge Transfer and Mass Transport in Metal-Assisted Chemical Etching of Silicon. *Sci. Rep.* **2016**, *6* (1), 36582.
(37) Zeis, R.; Lei, T.; Sieradzki, K.; Snyder, J.; Erlebacher, J. Catalytic Reduction of Oxygen and Hydrogen Peroxide by Nanoporous Gold. *J. Catal.* **2008**, *253* (1), 132–138.
(38) Andoralov, V. M.; Tarasevich, M. R.; Tripachev, O. V. Oxygen Reduction Reaction on Polycrystalline Gold. Pathways of Hydrogen Peroxide Transformation in the Acidic Medium. *Russ. J. Electrochem.* **2011**, *47* (12), 1327–1336.
(39) Flätgen, G.; Wasle, S.; Lübke, M.; Eickes, C.; Radhakrishnan, G.; Doblhofer, K.; Ertl, G. Autocatalytic Mechanism of H2O2 Reduction on Ag Electrodes in Acidic Electrolyte: Experiments and Simulations. *Electrochim. Acta* **1999**, *44* (25), 4499–4506.
(40) Li, Y.; Lenigk, R.; Wu, X.; Gruendig, B.; Dong, S.; Renneberg, R. Investigation of Oxygen- and Hydrogen Peroxide-Reduction on Platinum Particles Dispersed on Poly(o-Phenylenediamine) Film Modified Glassy Carbon Electrodes. *Electroanalysis* **1998**, *10* (10), 671–676.
(41) Huang, J. C.; Sen, R. K.; Yeager, E. Oxygen Reduction on Platinum in 85% Orthophosphoric Acid. *J. Electrochem. Soc.* **1979**, *126* (5), 786.
(42) Katsounaros, I.; Schneider, W. B.; Meier, J. C.; Benedikt, U.; Biedermann, P. U.; Auer, A. A.; Mayrhofer, K. J. J. Hydrogen Peroxide Electrochemistry on Platinum: Towards Understanding the Oxygen Reduction Reaction Mechanism. *Phys. Chem. Chem. Phys.* **2012**, *14* (20), 7384–7391.
(43) Fedynyshyn, T. H.; Grynkewich, G. W.; Hook, T. B.; Liu, M.-D.; Ma, T.-P. The Effect of Aluminum vs. Photoresist Masking on the Etching Rates of Silicon and Silicon Dioxide in CF4/O2 Plasmas. *J. Electrochem. Soc.* **1987**, *134* (1), 206–209.
(44) Fedynyshyn, T. H.; Grynkewich, G. W.; Ma, T.-P. Mask Dependent Etch Rates II. *J. Electrochem. Soc.* **1987**, *134* (10), 2580–2585.
(45) Fedynyshyn, T. H.; Grynkewich, G.; Dumas, R. H. Mask Dependent Etch Rates III. *J. Electrochem. Soc.* **1988**, *135* (1), 268–269.
(46) Fedynyshyn, T. H.; Grynkewich, G. W. The Effect of Metal Masks on the Plasma Etch Rate of Silicon. *J.Electrochem.Soc.* **1989**, *136* (6), 2–7.
(47) Kataoka, Y.; Shinmura, T.; Kanoh, M. Improvement in Downflow Etching Rate Using Au as a Catalyst. *J. Vac. Sci. Technol. A Vacuum, Surfaces, Film.* **2000**, *18* (2), 388.
(48) Selamoglu, N.; Mucha, J. A.; Flamm, D. L.; Ibbotson, D. E. Catalyzed Gaseous Etching of Silicon. *J. Appl. Phys.* **1987**, *62* (3), 1049–1053.
(49) Selamoglu, N.; Mucha, J. A.; Flamm, D. L.; Ibbotson, D. E. Copper-Catalyzed Etching of Silicon by F2: Kinetics and Feature Morphology. *J. Appl. Phys.* **1988**, *64* (3), 1494–1498.
(50) Dikarev, Y. I.; Surovtsev, I. S.; Tsvetkov, S. M. Catalytic Plasma Chemical Etching of Silicon and Silicon Dioxide. In *Proc. SPIE 5129, Fundamental Problems of Optoelectronics and Microelectronics*; 2003; pp 288–294.
(51) James, T.; Cho, J. H.; Fernandes, R.; Randhawa, J. S.; Gracias, D. H. A One-Step Etching Method to Produce Gold Nanoparticle Coated Silicon Microwells and Microchannels. *Anal. Bioanal. Chem.* **2010**, *398* (7–8), 2949–2954.
(52) James, T.; Kalinin, Y. V.; Chan, C. C.; Randhawa, J. S.; Gaevski, M.; Gracias, D. H. Voltage-Gated Ion Transport through Semiconducting Conical Nanopores Formed by Metal Nanoparticle-Assisted Plasma Etching. *Nano Lett.* **2012**, *12* (7), 3437–3442.
(53) Williams, K. R.; Gupta, K.; Wasilik, M. Etch Rates for Micromachining Processing-Part II. *J. Microelectromechanical Syst.* **2003**, *12* (6), 761–778.
(54) Madou, M. J. *Fundamentals of Microfabrication and Nanotechnology*, Third.; CRC Press, 2011.
(55) Jansen, H.; Gardeniers, H.; de Boer, M.; Elwenspoek, M.; Fluitman, J. A Survey on the Reactive Ion Etching of Silicon in Microtechnology. *J. Micromechanics Microengineering* **1996**, *6* (1), 14–28.

(56) D'Agostino, R.; Flamm, D. L. Plasma Etching of Si and SiO 2 in SF6 – O2 Mixtures. *J. Appl. Phys.* **1981**, *52* (1), 162–167.
(57) Mogab, C. J.; Adams, A. C.; Flamm, D. L. Plasma Etching of Si and SiO2 —The Effect of Oxygen Additions to CF 4 Plasmas. *J. Appl. Phys.* **1978**, *49* (7), 3796–3803.
(58) D'Agostino, R.; Cramarossa, F.; De Benedictis, S.; Ferraro, G. Spectroscopic Diagnostics of CF4-O2 Plasmas during Si and SiO2 Etching Processes. *J. Appl. Phys.* **1981**, *52* (3), 1259–1265.
(59) Vayenas, C. G.; Bebelis, S.; Ladas, S. Dependence of Catalytic Rates on Catalyst Work Function. *Nature* **1990**, *343*, 625–627.
(60) Biskupek, J.; Kaiser, U.; Falk, F. Heat- and Electron-Beam-Induced Transport of Gold Particles into Silicon Oxide and Silicon Studied by in Situ High-Resolution Transmission Electron Microscopy. *J. Electron Microsc. (Tokyo).* **2008**, *57* (3), 83–89.
(61) Fang, Y.; Jiang, Y.; Cherukara, M. J.; Shi, F.; Koehler, K.; Freyermuth, G.; Isheim, D.; Narayanan, B.; Nicholls, A. W.; Seidman, D. N.; et al. Alloy-Assisted Deposition of Three-Dimensional Arrays of Atomic Gold Catalyst for Crystal Growth Studies. *Nat. Commun.* **2017**, *8* (1), 2014.
(62) Fisher, D. J. *Diffusion in Silicon: 10 Years of Research*; Trans Tech Publication, 1998.
(63) Hubbard, K. J.; Schlom, D. G. Thermodynamic Stability of Binary Oxides in Contact with Silicon. *J. Mater. Res.* **1996**, *11* (11), 2757–2776.
(64) Harder, C.; Hammer, L.; Müller, K. Morphology Dependent Platinum Silicide Formation in Oxygen Ambient. *Phys. Status Solidi* **1994**, *146* (1), 385–392.
(65) Padiyath, R.; Seth, J.; Babu, S. V.; Matienzo, L. J. Deposition of Copper Films on Silicon Substrates: Film Purity and Silicide Formation. *J. Appl. Phys.* **1993**, *73* (5), 2326–2332.
(66) Hwang, I.-C.; Seppelt, K. Gold Pentafluoride: Structure and Fluoride Ion Affinity. *Angew. Chem. Int. Ed. Engl.* **2001**, *40* (19), 3690–3693.
(67) Mohr, F. The Chemistry of Gold-Fluoro Compounds: A Continuing Challenge for Gold Chemists. *Gold Bull.* **2004**, *37* (3–4), 164–169.
(68) Müller-Rösing, H.-C.; Schulz, A.; Hargittai, M. Structure and Bonding in Silver Halides. A Quantum Chemical Study of the Monomers: Ag 2 X, AgX, AgX 2 , and AgX 3 (X = F, Cl, Br, I). *J. Am. Chem. Soc.* **2005**, *127* (22), 8133–8145.
(69) *CRC Handbook of Chemistry and Physics*, 98th ed.; Rumble, J. R., Ed.; CRC Press, 2017.
(70) Wesendrup, R.; Schwerdtfeger, P. Structure and Electron Affinity of Platinum Fluorides. *Inorg. Chem.* **2001**, *40* (14), 3351–3354.

TOC Graphic: